A Modular Programmable Inorganic Cluster Discovery Robot for the Discovery and Synthesis of Polyoxometalates

Daniel S. Salley, Graham A. Keenan, De-Liang Long, Nicola L. Bell, and Leroy Cronin*

Cite This: https://dx.doi.org/10.1021/acscentsci.0c00415
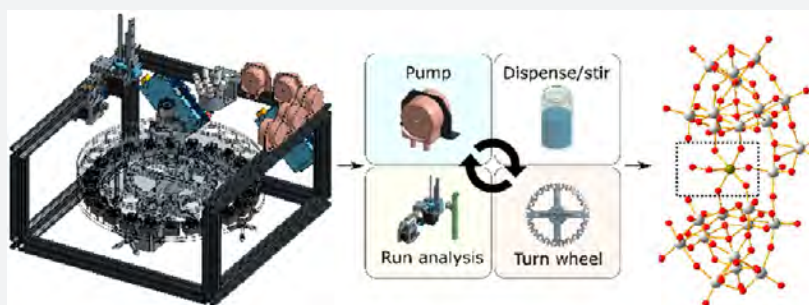
Read Online

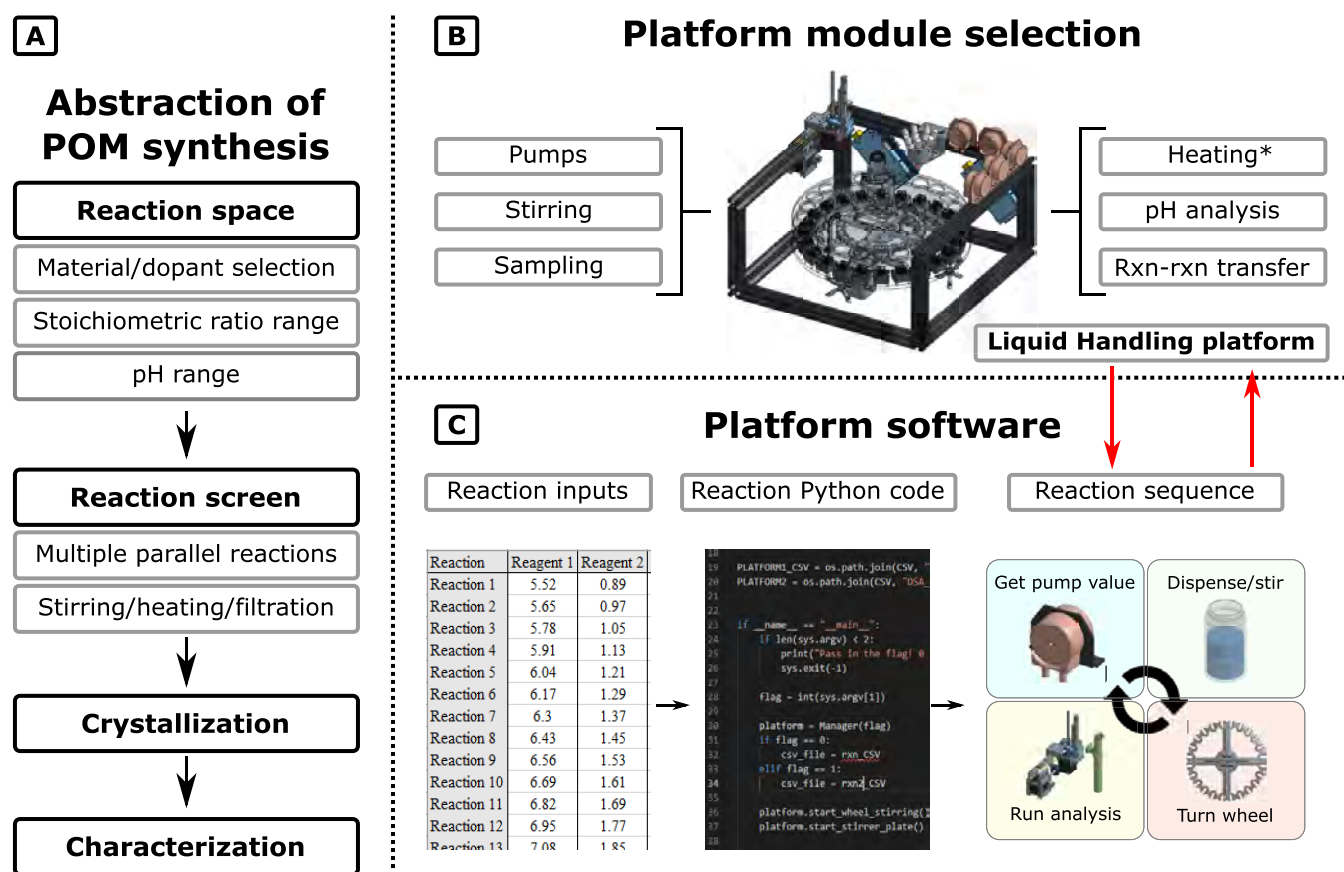ACCESS | 📊 Metrics & More | 📖 Article Recommendations | SI Supporting Information

ABSTRACT: The exploration of complex multicomponent chemical reactions leading to new clusters, where discovery requires both molecular self-assembly and crystallization, is a major challenge. This is because the systematic approach required for an experimental search is limited when the number of parameters in a chemical space becomes too large, restricting both exploration and reproducibility. Herein, we present a synthetic strategy to systematically search a very large set of potential reactions, using an inexpensive, high-throughput platform that is modular in terms of both hardware and software and is capable of running multiple reactions with in-line analysis, for the automation of inorganic and materials chemistry. The platform has been used to explore several inorganic chemical spaces to discover new and reproduce known tungsten-based, mixed transition-metal polyoxometalate clusters, giving a digital code that allows the easy repeat synthesis of the clusters. Among the many species identified in this work, the most significant is the discovery of a novel, purely inorganic $W_{24}Fe^{III}$−superoxide cluster formed under ambient conditions. The modular wheel platform was employed to undertake two chemical space explorations, producing compounds **1**−**4**: $(C_2H_8N)_{10}Na_2[H_6Fe(O_2)W_{24}O_{82}]$ (**1**, $\{W_{24}Fe\}$), $(C_2H_8N)_{72}Na_{16}[H_{16}Co_8W_{200}O_{660}(H_2O)_{40}]$ (**2**, $\{W_{200}Co_8\}$), $(C_2H_8N)_{72}Na_{16}[H_{16}Ni_8W_{200}O_{660}(H_2O)_{40}]$ (**3**, $\{W_{200}Ni_8\}$), and $(C_2H_8N)_{14}[H_{26}W_{34}V_4O_{130}]$ (**4**, $\{W_{34}V_4\}$), along with many other known species, such as simple Keggin clusters and 1D $\{W_{11}M^{2+}\}$ chains.

■ INTRODUCTION

Exploring the self-assembly and synthesis of high-nuclearity inorganic clusters is challenging, as many new chemical procedures are not always reproducible, and the new compounds are often produced in a very low yield.[1] Automation offers a solution that allows the digital control of liquid handling as a function of the reaction methodology. Indeed, automated reactor platforms have been used for the synthesis of nanoparticles,[2] clusters[3] and porous materials.[4] Despite this, an ongoing challenge is to design automated arrays of experiments to allow both the exploration and understanding of the chemical space.[5−7] As such, the use of a multiplexed approach to sample large compositional arrays (LCAs) is a valuable strategy since it allows the rapid exploration and identification of potential discovery areas in a digital and reproducible manner. Molecular metal oxides or polyoxometalates (POMs) are one such family of inorganic clusters with nuclearities ranging from 6 to over 360 metal centers. POMs are traditionally formed by group 5 or 6 transition metals (V, Nb, Ta, Mo, and W) in their highest

oxidation states, typically synthesized in one pot and purified via crystallization.[8] POMs have attracted great attention in recent decades for their unique structural properties[9] and potential application in a number of fields, including medicine,[10] catalysis,[11] and materials chemistry.[12] More recently, examples of POMs being used as high-density electron storage media have been reported, revealing the potential use for these compounds in the growing global need for easily accessible energy storage.[13] By combining metal−oxo moieties with heteroanions, such as SO_4^{2-}, PO_4^{3-}, and AsO_4^{3-}, and transition-metal ions, such as Co^{2+}, Fe^{3+}, etc., the stability and structural diversity of the clusters is increased.[14] These

A

Abstraction of POM synthesis

Reaction space

Material/dopant selection

Stoichiometric ratio range

pH range

⬇

Reaction screen

Multiple parallel reactions

Stirring/heating/filtration

⬇

Crystallization

⬇

Characterization

B

Platform module selection

Pumps

Stirring

Sampling

Heating*

pH analysis

Rxn-rxn transfer

Liquid Handling platform

C

Platform software

Reaction inputs

Reaction Python code

Reaction sequence

Reaction	Reagent 1	Reagent 2
Reaction 1	5.52	0.89
Reaction 2	5.65	0.97
Reaction 3	5.78	1.05
Reaction 4	5.91	1.13
Reaction 5	6.04	1.21
Reaction 6	6.17	1.29
Reaction 7	6.3	1.37
Reaction 8	6.43	1.45
Reaction 9	6.56	1.53
Reaction 10	6.69	1.61
Reaction 11	6.82	1.69
Reaction 12	6.95	1.77
Reaction 13	7.08	1.85

Get pump value   Dispense/stir

Run analysis   Turn wheel

Figure 1. (A) Abstraction of inorganic/polyoxometalate synthesis. (B) The MWP is built using modules selected by the user to perform the required operation (*heating performed using an auxiliary module, see SI, section 1.2). (C) Reaction inputs via CSV/JSON files communicate with the hardware from an executable synthesis code, all handled by our in-house software.

units can then be linked by transition heterometals (M), such as Co, V, Ni, Mn, and Fe, allowing building blocks (BBs) with unique structural features to be formed.[9,15] Furthermore, we have recently shown that the exploration of crystallization can be done using active-learning with automated systems, opening up the prospect of developing intelligent search systems that explore supramolecular chemistry.[16]

Automation is ideal for the one-pot synthetic procedure involved in most POM syntheses; however, there are currently only two options available to the chemist when automating any process: (1) to incur significant expense by purchasing proprietary hardware and software or (2) to create bespoke technology that can often expire in its utility at the end of the project, despite having required significant resources and expertise to create, test, and implement. To provide a more accessible alternative, we sought to create an inexpensive, modular device capable of performing the basic tasks needed for simple to moderate-complexity laboratory work. Herein, we describe the development of a modular parallelized reactor platform and its application to explore inorganic parameter space efficiently and reliably, leading to the discovery of new clusters using digital code. Importantly, the digitization of the search process allowed for the highly accurate control of the reaction parameters, via the automated hardware, which led to these discoveries, allowing for consistent repeatability and subsequent optimization. This is vital, as newly discovered structural motifs are often isolated in low yields with only a narrow window of "synthetic coordinates". Using this automated platform, we have identified 3 new mixed

transition-metal W species and the reproducible synthesis of $\{W_{200}Co_8\}$, the largest W-based POM known, built of four $\{W_{49}M\}$ (M = Co, Ni) fragments, each bridged in a wheel-like structure by one $\{WO_6\}$ and one $\{MO_6\}$ unit. This structure in particular is difficult to synthesis and, as such, seemed to suffice as an appropriate challenge for the platform as part of the project. Each of these compounds were isolated by crystallization and, most importantly, could be readily reproduced using our modular wheel platform.

■ RESULTS AND DISCUSSION

Platform Design. The modular wheel platform (MWP) presented herein is a liquid handling device that uses a combination of custom designed parts (either 3D-printed or fabricated in-house), commercially available components, and in-house open-source software, of which details for reproduction are provided in the Supporting Information (SI). Our platform design allows for the addition and modification of functions as needed and was used, in this instance, to explore an inorganic chemical space in a high-throughput and reproducible manner. Figure 1 outlines the abstraction of the processes needed for this chemistry (A), in addition to the platform's hardware (B) and software (C). In general, the inorganic synthesis space can be traversed by the modification of reagents used, relative ratios, concentration, and solution pH. Parallelization allows for high-throughput reactivity screening, increasing the potential for discovery while minimizing time constraints, to allow for rapid feedback. Additional modulation of reactivity can then be provided by
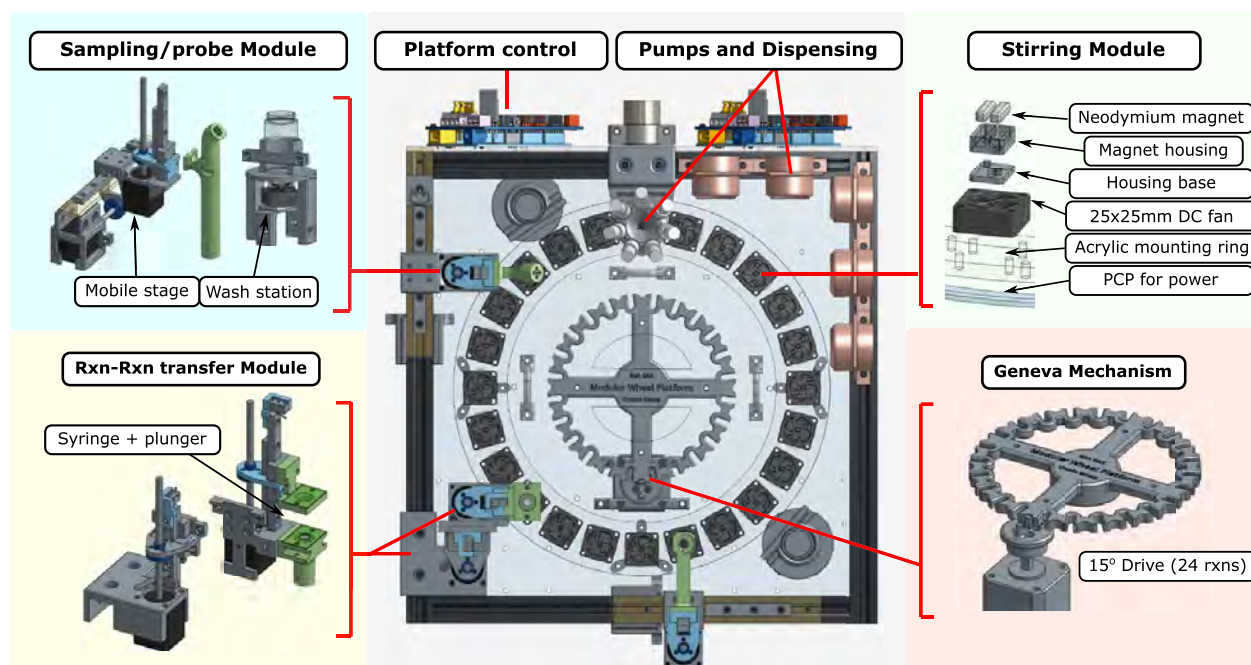
Figure 2. Top view of a modular wheel platform, equipped with numerous modules and accompanying functions. Detailed descriptions of these individual modules can be found in SI, section 1.2.

stirring or heating, with discoveries in the search space identified by crystallization. The automation of these fundamental synthetic processes, controlled by digital code and combined with the plug-and-play functionality of the platform, is designed to provide the MWP with wide-ranging utility.

The base unit of the MWP, capable of running 24 parallel reactions, can be assembled in 5−6 h (Figure 2). A Geneva wheel mechanism allows the platform to dispense 24 sequential reaction mixtures via high-accuracy peristaltic pumps, with each reactor individually stirred by a custom magnetic stirring module. A series of compact and standalone modules capable of x, y, and z movement along the platform frame have been developed, allowing for in-line measurements of the probe-based feedback, sample extraction for analyses, and transfer between vials. Standalone multireaction heating/stirring and filtration modules were also developed as part of the workflow (see SI, section 1.2). All custom hardware is controlled using an Arduino Mega2650 via in-house, open-source software designed with the same modular approach in mind.

Digital Code. Converting the synthesis of inorganic clusters into digital code essentially creates an executable series of operations that can be performed on any given hardware workflow that has the appropriate functions (SI, Figure 1.11). In our case, this involves converting steps such as dispensing reagents, general stepper motor control, pH recording, etc. into an executable digital code for each reaction. As chemical discoveries are made, this digital code becomes far more than a series of mechanical operations, it is then a reproducible means of forming these new discoveries. Ultimately, that was the goal of this work: to create a digital executable reaction code that can be implemented anywhere in order to be able to reproduce discoveries (SI, Figure 1.12).

Automated Inorganic Synthesis. The Modular Wheel Platform (MWP) was employed to undertake the exploration

of two different chemical spaces, producing compounds **1**−**4**: $(C_2H_8N)_{10}Na_2[H_6Fe(O_2)W_{24}O_{82}]$ (**1**, $\{W_{24}Fe\}$), $(C_2H_8N)_{72}Na_{16}[H_{16}Co_8W_{200}O_{660}(H_2O)_{40}]$ (**2**, $\{W_{200}Co_8\}$), $(C_2H_8N)_{72}Na_{16}[H_{16}Ni_8\ W_{200}O_{660}(H_2O)_{40}]$ (**3**, $\{W_{200}Ni_8\}$), and $(C_2H_8N)_{14}[H_{26}W_{34}V_4O_{130}]$ (**4**, $\{W_{34}V_4\}$), along with many other known species, e.g., simple Keggin clusters and 1D $\{W_{11}M^{2+}\}$ chains.

Space 1 consisted of 60 reactions, all with constant volumes of aqueous stock solutions of sodium tungstate (Na_2WO_4, 0.723 M, 5 mL), dimethylamine hydrochloride (DMA·HCl, 2.43 M, 4 mL), hydrochloric acid (HCl, 0.5 M, 0.1 mL), and sodium dithionite ($Na_2S_2O_4$, 0.5 M, 0.73 mL), while varying the contributions of four transition-metal solutions of Fe^{2+}, Co^{2+}, Ni^{2+}, and Mn^{2+} (0.5 M, 0.0875−0.425 mL). All reactions performed on this MWP total between 10 and 13 mL in volume, which has the advantage of utilizing economical reagent use while ensuring sufficient product formation for analysis, despite low relative precentage yields. In order to systematically investigate the reaction system generated by these four MCl_2 stock solutions, we considered the parameter space in three dimensions containing all the possible compositions and combinations. The six edges of this tetrahedral space give the binary combinations (M_1/M_2), four faces tertiary combinations ($M_1/M_2/M_3$), and the inner volume quaternary combinations ($M_1/M_2/M_3/M_4$). This approach allowed us to generate a two-dimensional array in the following combinations: Co^{2+}/Ni^{2+}, Mn^{2+}/Co^{2+}, Ni^{2+}/Fe^{2+}, Fe^{2+}/Mn^{2+}, and $Co^{2+}/Ni^{2+}/\ Mn^{2+}/Fe^{2+}$. This 2D representation is for simplicity in picturing the 60 reactions performed while the 3D tetrahedron accurately represents the solution compositions. Both representations of space 1 and the MWP itself are shown in Figure 3.

Space 1 resulted in a range of unique formations represented by complexes **1**−**3**, ranging from simple Keggin structures to gigantic $\{W_{200}M_8\}$ clusters. The most significant discovery of this space to date has been the formation complex **1**,
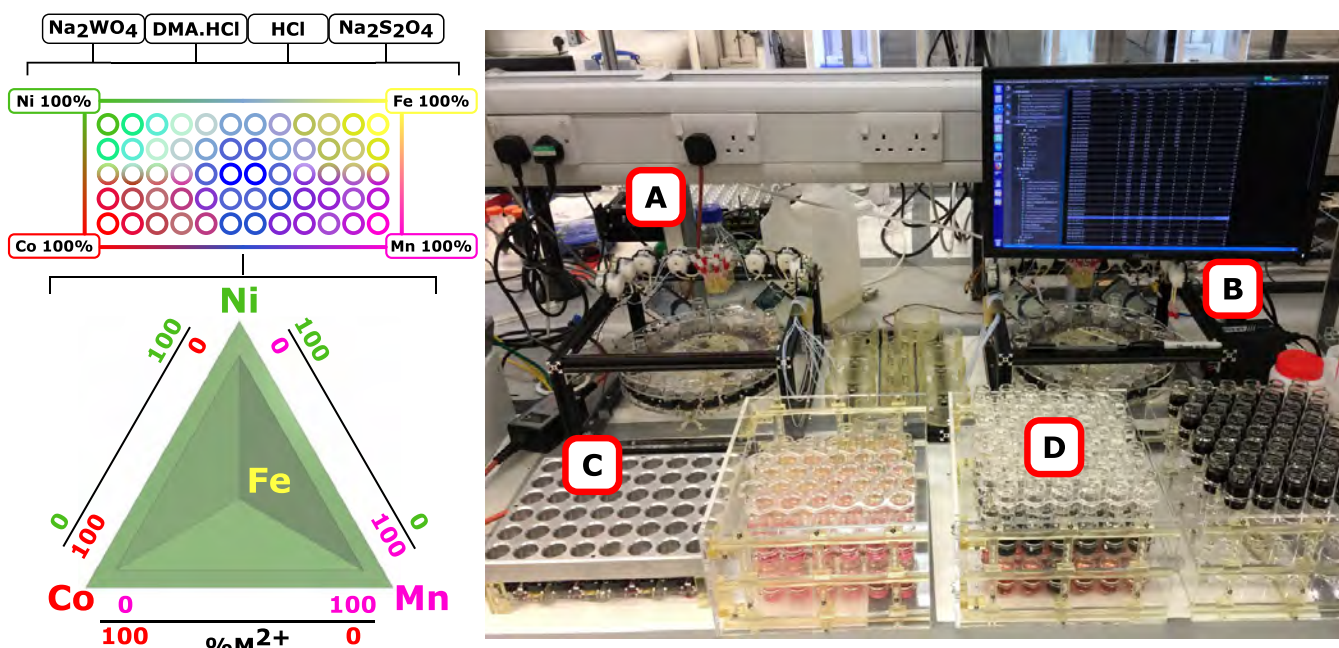
Figure 3. Space 1 2D and 3D representations (top left and bottom left respectively): (A) modular wheel platform, (B) PC and platform power supply, (C) accompanying heating stirring mantle, and (D) reaction samples storage for crystallization.

containing a stable $Fe^{3+}-O-O$ superoxide moiety, bridging two $\{W_{11}\}$ fragments (Figure 4). The cluster forms as large growths of overlaying light-yellow cuboid crystals (SI, section 2.2.3, Figures 2.1A and 2.2G) at between pH 2.50−3.15. The highest yield to date of this reaction has been 192 mg (10.59% based on W). When attempting to optimize/repeat this reaction, it was found that, compared to other examples in this work, this reaction is relatively insensitive to pH but highly sensitive to $FeCl_2$ concentration, and by the reducing the agent stoichiometry, a slight deviation of their relative ratios failed to produce this cluster. In fact, upon purchasing fresh batches of $Na_2S_2O_4$ and $FeCl_2 \cdot 4H_2O$, lowering both of their relative ratios was required to achieve continued reproducibility, demonstrating the sensitivity of these conditions to reagent purity (SI, section 2.1.5). An μ_{eff} of 5.83 μB for the Fe center, determined by Evans method ^1H NMR spectroscopy, reveals a high-spin d^5 state indicative of a Fe^{3+} center (see SI, section 2.4). Thus, the oxidation of the original Fe^{2+} source under reducing conditions, combined with an O−O bond length of 1.245 Å and the characteristic signal bands for O−O at $v = 967$ cm^{-1} by Raman and $v = 1013$ cm^{-1} by IR spectroscopies, confirms the formation of a superoxide,[17,18] presumably from atmospheric oxygen. The mechanism of this change is likely similar to the binding of oxygen in hemoglobin.[19] Superoxide formation on a POM has been proposed as an intermediate step of an O_2 activation process in $[Ru^{3+}_2(OH)_2(H_2O)_2SiW_{10}O_{36}]^{4-}$ by Kuznetsov et al.,[20] and a single example of a POM enhancing the oxidative power of a mixed zerovalent iron nanoparticle/ferrous ion solution in the presence of O_2 has been reported.[21] However, to the best of our knowledge, this cluster is a unique example of an end-on (η^1) Fe−superoxide embedded in a tungsten oxide framework, formed under mild conditions and stable for months in the solid state.

Also discovered in space 1 were samples of $\{W_{200}M_8\}$ containing Co^{2+} and Ni^{2+}, forming in numerous reactions at rather unexpected positions in the space. We have previously reported the isolation of $\{W_{200}Co_8\}$; however, this robotic

discovery represents the first time the nickel analogue has been observed.[22] This structure requires between 4 and 10 weeks of crystallization time, and the products are typically produced in very low yield, meaning many samples containing these compounds can become contaminated with crystals of starting materials or alternative, higher-yielding products. This phenomenon ranged from samples containing barely 10 crystals with up to three other products present to vials containing $\{W_{200}M_8\}$ as the sole product in relatively high yields given its rarity and size. One fortunate attribute of this compound is that well-formed crystals of the cluster have a highly distinctive serrated star shape (see SI, Figure 2.1B and C), making the initial indication of its presence over time easier to observe. In this space, 14 of the 60 reactions produced $\{W_{200}M_8\}$ (M = Co or Ni) in varying purities and yields, with **2** (M = Co) representing the majority of these samples.

For each compound, samples producing the highest yield and purity were selected for analysis. The most successful reaction conditions for the formation of the Co-containing cluster $\{W_{200}Co_8\}$ **2** was at the specific $[Co^{2+}]:[Ni^{2+}]:[Mn^{2+}]:[Fe^{2+}]$ ratio of 49.3:10.9:34.3:5.5 at an initial pH of 2.2. This reaction produced a yield of 87 mg (4.1% based on W) with the $\{W_{200}Co_8\}$ crystals being the sole formation, a rare occurrence. The crystal structure of compound **2** revealed the $\{W_{200}\}$ nanosized framework constructed by tungsten-based $\{W_{49}M\}$ building blocks. For $\{W_{200}Ni_8\}$ **3**, the binary combination of $[Ni^{2+}]:[Fe^{2+}]$ at 79.5:20.5 produced the best results. Marginally different in crystal appearance to the pale red/orange crystals of compound **2**, these yellow crystals begin as pentagonal plate-like growths, one face being concave with a star pattern radiating from the center and the other being a convex bowl-like shape. Over a period of two months, some of these crystals grew out from the pentagonal edges, into a distorted star shape with the same serrated edges as seen in the Co example (see SI, section 2.2.3, for crystal images). The highest yield of this compound was very low (17 mg, 0.8% based on W) but sufficient for analysis. Intriguingly, we have
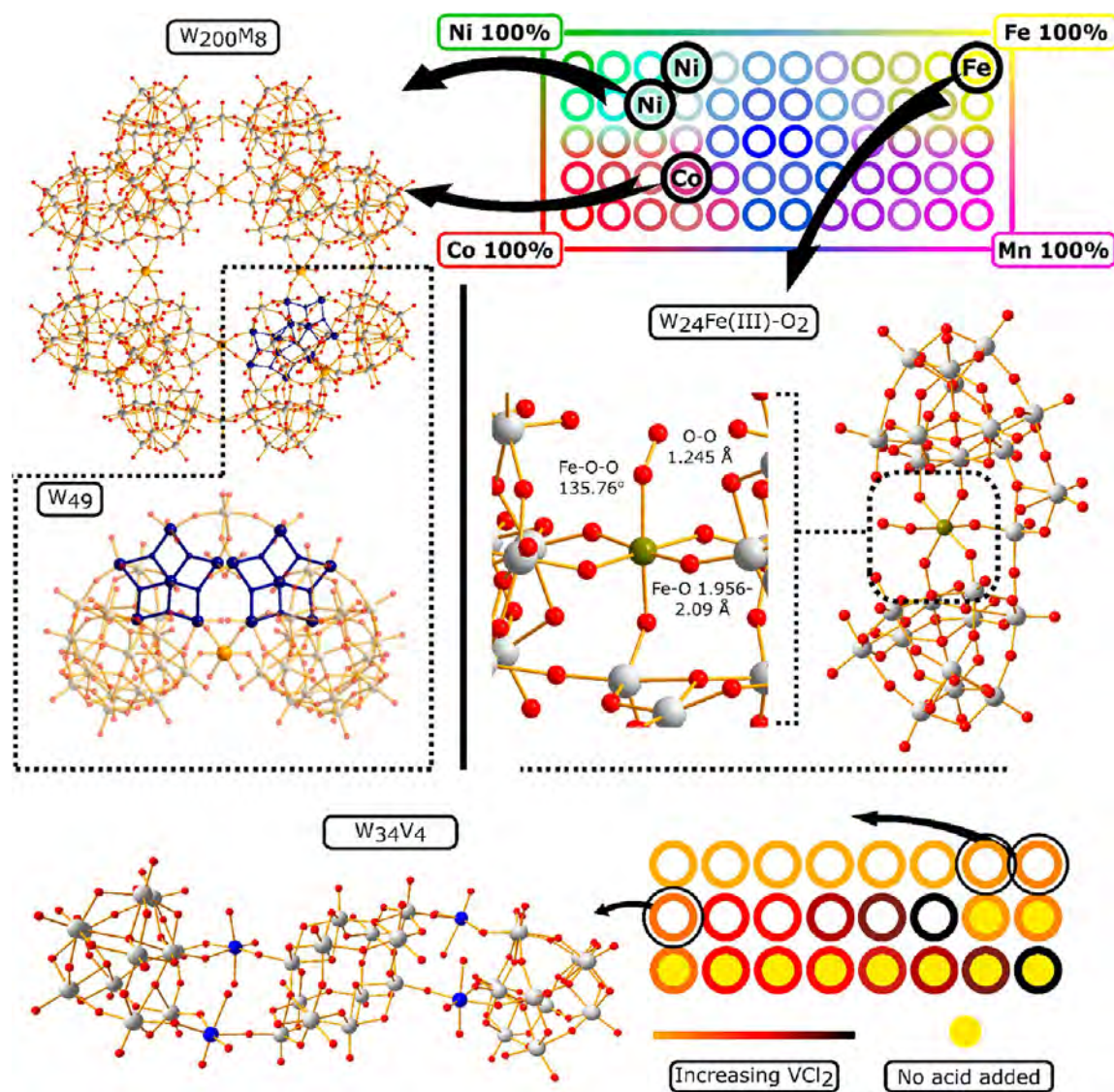
Figure 4. Mixed W/M space search and compound discovery locations (top right). $W_{200}M_8$/$W_{49}M$ **2**/**3** structures (top-left). $W_{24}Fe$ **1** superoxide cluster and detailed view of Fe^{3+}−superoxide center (middle/right). $W_{34}V_4$ **4** structure and reaction space (bottom).

not yet been able to isolate either compound **1** or **2** from solutions containing only a single heterometal ion in solution.

Continuing from the initial success of space 1, space 2 was identical in the contribution of tungstate, reducing agent, and DMA, while exploring the influence of pH and introducing V^{2+} as the heterotransition metal ion. The space consisted of 24 reactions and produced $\{W_{34}V^{4+}_4\}$ **4** (Figure 4 bottom). The characteristic initial blue color faded over a period of 2 h at RT, and the remaining brown/black, opaque mixtures filtered simultaneously using the filtration array (see SI, section 1.2.7). Black needle-shaped crystals formed in low/moderate yields within 2 weeks in 3 of the 24 samples as the initial pH proceeded toward 2.20. The highest yielding sample produced just 21 mg (1.12% based on W) of pure product. This yield is mainly due to the difficulty in isolation of the small needles from other crystallized products (mainly Na_2WO_4). The significant pH difference from the reactions in space 1 was due mainly to the presence of VCl_2. Increasing the stoichiometry of VCl_2 further resulted in pH values <2.0, and little or no formation of the compound was observed. This shows a narrow window of pH in which **4** is produced between

2.20 and 2.75. The structure forms a §-shape between three distinct fragments, two terminal $\{W_{11}\}$ and a central $\{W_{12}\}$ cage via VO_6 linkages. The V^{2+} source undergoes expected oxidation in air to produce V^{4+} with both terminal V=O and bridging V−O−W bonds, shown clearly in the crystallographic data. All bridging VO_6 structures therefore have a distorted octahedral geometry, allowing for the unequal arrangement of bonding between the central and terminal fragments, the central cage being bound to the V centers via a single η^2 V−O−W bond and the terminal $\{W_{11}\}$ fragments bound by two η^3 V−[O−W]$_2$ bridges.

Compounds **1** and **4** are similar to the $\{W_{22}\}$ and $\{W_{34}\}$ iso-polyoxotungstate species published by our group in 2008, with the W−O−W linkages between distinct W-subunits being replaced fully or in part by heterometal-oxo linkages.[23] For compound **1**, the two $\{W_{11}\}$ subunits are essentially mirror images of one another across two bridging tungsten atoms and the central Fe atom, forming a flexible cavity for the Fe position as opposed to the S-shape made by the same subunits in this previous paper. Compound **4**, however, is remarkably similar to the $\{W_{34}\}$ iso-polyoxotungstate. In that paper, we

theorized that the lacunary positions on the $\{W_{11}\}$ subunits present in these compounds could offer opportunities to further increase the structural diversity of this class of molecules, and the work described herein is the first example, to our knowledge, of the realization of that hypothesis.

CONCLUSIONS

We have created a high-throughput, inexpensive modular platform for the exploration of an inorganic synthesis space and have utilized this device in the discovery of new metal oxide clusters. These discoveries, made between narrow windows in the chemical space, could easily have been missed or proved irreproducible during bench synthesis. Most notable is the discovery of the first stable POM–superoxide species, synthesized under mild conditions, within such a heavily explored chemical space. The fact that mixed transition-metal W-based POM synthesis has been studied for decades and yet the simple synthesis of this novel structure remained unobserved until now shows the utility of this robotic system. The medium-scale batch approach of systematic chemical space exploration allowed for the reproducible synthesis and crystallization of these systems, while the platform's accuracy and efficiency allowed for extensive exploration of the chemistry selected for investigation, as well as mapping of the fine boundaries between crystal formation and failure with minimal effort. In the near future, we intend to add greater functionality to this modular architecture, advancing its liquid handling capabilities and incorporating multiple sensor types. Our immediate intention is to integrate spectroscopic capabilities, centered around the modular wheel platform, that can provide direct reaction feedback to create closed-loop systems working autonomously. With this direct access to reaction feedback, we hope to incorporate the use of algorithms in the decision-making process for future reaction conditions, a method that has shown such promise in other reported works.[24,25]

EXPERIMENTAL SECTION

Safety Statement. No unexpected or unusually high safety hazards were encountered during this work.

Synthesis of Compounds 1–4. Full details of the platform hardware and software can be found in the SI, section 1, and in the open-source repository (https://github.com/croningp/InorganicClusterDiscovery).

Synthesis of compounds **1–4** proceeded by the following sequence. Aqueous stock solutions were dispensed in the following order: (1) sodium tungstate (0.66 M adjusted to pH 3 using conc. HCl), (2) dimethylamine hydrochloride $(CH_3)_2NH \cdot HCl$ (2.453 M), (3) hydrochloric acid (0.5 M), (4) sodium dithionite $Na_2S_2O_4$ (0.5 M), and (5) up to four transition-metal solutions [0.5 M]. Full reaction grids can be found in the SI, section 2. Reactions were stirred at ca. 800 rpm for 1–2 h in a 14 mL disposable glass vial and vacuum filtered using the filtration array through polytetrafluoroethylene frits/filter paper. Crystallization times varied from 1 week to 2 months (see SI).

Further experimental procedures and compound characterization can be found in the SI, section 2.

Compound 1, $Na_2(C_2H_8N)_{10}[H_6W_{24}Fe(O_2)O_{82}] \cdot 20H_2O.$ $C_{20}H_{126}FeN_{10}Na_2O_{104}W_{24}$; M_r = 6685.53 g·mol^{-1}; yellow block crystals; triclinic; space group, $P\bar{1}$; a = 13.1545(16), b = 18.807(2), c = 25.522(3) Å; α = 104.421(2), β =

104.482(2), γ = 96.678(2)°; V = 5812.3(12) Å^3; Z = 2; ρ = 3.820 Mg·m^{-3}; λ Mo Kα = 0.71073 Å; 197690 reflections measured; 22842 unique reflections ($R_{(int)}$ = 0.0365), which were used in all calculations; 1379 refined parameters; final R1 = 0.0300, wR2 = 0.0711 (all data); Raman O–O superoxide peak, 967 cm^{-1} (s). Elemental analysis calculated (%): W (65.88), Fe (0.87), C (3.59), H (1.9), N (2.11). Found (%): W (65.58), Fe (0.92), C (4.06), H (1.81), N (2.28). Average yield across 5 repeat reactions: 0.104 g (9% based on W).

Compound 2. Compound **2** reproduced from a previous work (CSD 895471).[22]

Compound 3, $Na_{16}(C_2H_8N)_{72}[H_{16}W_{200}Ni_8O_{660}(H_2O)_{40}] \cdot$ $450H_2O.$ $C_{144}H_{1572}Ni_8N_{72}Na_{16}O_{1150}W_{200}$; M_r = 60330.16 g·mol^{-1}; yellow serrated star shaped crystals (see SI, section 2.2.3, crystal images); tetragonal; space group, $P42/nmc$; a = 48.8657(4), c = 29.4123(2) Å; V = 70232.4(7) Å^3; Z = 2; ρ = 2.786 Mg·m^{-3}; λ Mo Kα = 0.71073 Å; 383669 reflections measured; 33492 unique reflections ($R_{(int)}$ = 0.0711), which were used in all calculations; 1132 refined parameters; final R1 = 0.0677, wR2 = 0.195 (all data). Elemental analysis calculated (%): W (60.94), Ni (0.778), C (2.86), H (2.62), N (1.67). Found (%): W (63.02), Ni (0.765), C (3.3), H (1.45), N (1.63). Average yield across 5 repeat reactions: 9 mg (0.45% based on W).

Compound 4, $(C_2H_8N)_{14}[H_{26}W_{34}V_4O_{130}] \cdot 30H_2O.$ $C_{28}H_{202}V_4N_{14}O_{164}W_{34}$; M_r = 9782.68 g·mol^{-1}; black needle crystals; triclinic; space group, $P\bar{1}$; a = 13.5219(16), b = 18.592(2), c = 20.285(2) Å; α = 68.689(2), β = 79.219(2), γ = 75.283(2)°; V = 4569.5(9) Å^3; Z = 1; ρ = 3.555 Mg·m^{-3}; λ Mo Kα = 0.71073 Å; 57247 Reflections measured; 17941 unique reflections ($R_{(int)}$ = 0.0516), which were used in all calculations; 976 refined parameters; final R1 = 0.0421, wR2 = 0.1197 (all data). Elemental analysis calculated (%): W (62.18), V (2.03), C (3.52), H (1.75), N (2.05). Found (%): W (61.67), V (2.114), C (3.91), H (1.4), N (2.14). Average yield across 5 repeat reactions: 14 mg (0.74% based on W).

ASSOCIATED CONTENT

ⓢ Supporting Information

The Supporting Information is available free of charge at https://pubs.acs.org/doi/10.1021/acscentsci.0c00415.

> The Supporting Information contains the following: A detailed hardware and software description of the modular wheel platform (MWP), including additional modules; a GitHub repository link for the hardware construction, STL files for 3D prints, DWG files for laser cuts, software installation/usage guide, and a bill of materials; and a detailed description of the chemistry performed using the platform, including material sources, stock solutions preparations, experimental parameters for the chemical space exploration, and full analytical data for compounds **1–4**, including XRD tables and crystal photographs (PDF)

AUTHOR INFORMATION

Corresponding Author

Leroy Cronin — *School of Chemistry, The University of Glasgow, Glasgow G12 8QQ, United Kingdom;* ⓞ orcid.org/0000-0001-8035-5757; Email: lee.cronin@glasgow.ac.uk

Authors

Daniel S. Salley − *School of Chemistry, The University of Glasgow, Glasgow G12 8QQ, United Kingdom*

Graham A. Keenan − *School of Chemistry, The University of Glasgow, Glasgow G12 8QQ, United Kingdom*

De-Liang Long − *School of Chemistry, The University of Glasgow, Glasgow G12 8QQ, United Kingdom;* ⦿ orcid.org/0000-0003-3241-2379

Nicola L. Bell − *School of Chemistry, The University of Glasgow, Glasgow G12 8QQ, United Kingdom;* ⦿ orcid.org/0000-0002-7497-9667

Complete contact information is available at:
https://pubs.acs.org/10.1021/acscentsci.0c00415

■ REFERENCES

(1) Malakoutikhah, M.; Peyralans, J. J. P.; Colomb-Delsuc, M.; Fanlo-Virgos, H.; Stuart, M. C. A.; Otto, S. Uncovering the Selection Criteria for the Emergence of Multi-Building-Block Replicators from Dynamic Combinatorial Libraries. *J. Am. Chem. Soc.* **2013**, *135* (49), 18406−18417.

(2) Mirhosseini Moghaddam, M.; Baghbanzadeh, M.; Sadeghpour, A.; Glatter, O.; Kappe, C. O. Continuous-Flow Synthesis of CdSe Quantum Dots: A Size-Tunable and Scalable Approach. *Chem. - Eur. J.* **2013**, *19* (35), 11629−11636.

(3) Richmond, C. J.; Miras, H. N.; de la Oliva, A. R.; Zang, H.; Sans, V.; Paramonov, L.; Makatsoris, C.; Inglis, R.; Brechin, E. K.; Long, D.-L.; Cronin, L. A flow-system array for the discovery and scale up of inorganic clusters. *Nat. Chem.* **2012**, *4* (12), 1037−1043.

(4) Rubio-Martinez, M.; Batten, M. P.; Polyzos, A.; Carey, K. C.; Mardel, J. I.; Lim, K. S.; Hill, M. R. Versatile, High Quality and Scalable Continuous Flow Production of Metal-Organic Frameworks. *Sci. Rep.* **2015**, *4* (1), 5443.

(5) Vila-Nadal, L.; Cronin, L. Design and synthesis of polyoxometalate-framework materials from cluster precursors. *Nat. Rev. Mater.* **2017**, *2* (10), 17054.

(6) Yoshida, J.; Takahashi, Y.; Nagaki, A. Flash chemistry: flow chemistry that cannot be done in batch. *Chem. Commun.* **2013**, *49* (85), 9896−9904.

(7) Parrott, A. J.; Bourne, R. A.; Akien, G. R.; Irvine, D. J.; Poliakoff, M. Self-Optimizing Continuous Reactions in Supercritical Carbon Dioxide. *Angew. Chem., Int. Ed.* **2011**, *50* (16), 3788−3792.

(8) Vila-Nadal, L.; Rodriguez-Fortea, A.; Yan, L. K.; Wilson, E. F.; Cronin, L.; Poblet, J. M. Nucleation Mechanisms of Molecular Oxides: A Study of the Assembly-Dissassembly of $[W_6O_{19}]^{2-}$ by Theory and Mass Spectrometry. *Angew. Chem., Int. Ed.* **2009**, *48* (30), 5452−5456.

(9) Miras, H. N.; Yan, J.; Long, D. L.; Cronin, L. Engineering polyoxometalates with emergent properties. *Chem. Soc. Rev.* **2012**, *41* (22), 7403−7430.

(10) Rhule, J. T.; Hill, C. L.; Judd, D. A.; Schinazi, R. F. Polyoxometalates in medicine. *Chem. Rev.* **1998**, *98* (1), 327−357.

(11) Wang, S. S.; Yang, G. Y. Recent Advances in Polyoxometalate-Catalyzed Reactions. *Chem. Rev.* **2015**, *115* (11), 4893−4962.

(12) Wang, S. M.; Hwang, J.; Kim, E. Polyoxometalates as promising materials for electrochromic devices. *J. Mater. Chem. C* **2019**, *7* (26), 7828−7850.

(13) Chen, J. J.; Symes, M. D.; Cronin, L. Highly reduced and protonated aqueous solutions of $[P_2W_{18}O_{62}]^{6-}$ for on-demand hydrogen generation and energy storage. *Nat. Chem.* **2018**, *10* (10), 1042−1047.

(14) Zang, H. Y.; de la Oliva, A. R.; Miras, H. N.; Long, D. L.; McBurney, R. T.; Cronin, L. Discovery of gigantic molecular nanostructures using a flow reaction array as a search engine. *Nat. Commun.* **2014**, *5* (1), 3715.

(15) Smith, R. D. L.; Prevot, M. S.; Fagan, R. D.; Trudel, S.; Berlinguette, C. P. Water Oxidation Catalysis: Electrocatalytic Response to Metal Stoichiometry in Amorphous Metal Oxide Films Containing Iron, Cobalt, and Nickel. *J. Am. Chem. Soc.* **2013**, *135* (31), 11580−11586.

(16) Duros, V.; Grizou, J.; Xuan, W. M.; Hosni, Z.; Long, D. L.; Miras, H. N.; Cronin, L. Human versus Robots in the Discovery and Crystallization of Gigantic Polyoxometalates. *Angew. Chem., Int. Ed.* **2017**, *56* (36), 10815−10820.

(17) Cramer, C. J.; Tolman, W. B.; Theopold, K. H.; Rheingold, A. L. Variable character of O-O and M-O bonding in side-on (η^2) 1:1 metal complexes of O_2. *Proc. Natl. Acad. Sci. U. S. A.* **2003**, *100* (7), 3635−3640.

(18) Fukuzumi, S.; Lee, Y. M.; Nam, W. Structure and reactivity of the first-row d-block metal-superoxo complexes. *Dalton Trans.* **2019**, *48*, 9469−9489.

(19) Paoli, M.; Liddington, R.; Tame, J.; Wilkinson, A.; Dodson, G. Crystal structure of T state haemoglobin with oxygen bound at all four haems. *J. Mol. Biol.* **1996**, *256* (4), 775−792.

(20) Kuznetsov, A. E.; Geletii, Y. V.; Hill, C. L.; Morokuma, K.; Musaev, D. G. Dioxygen and Water Activation Processes on Multi-Ru-Substituted Polyoxometalates: Comparison with the "Blue-Dimer" Water Oxidation Catalyst. *J. Am. Chem. Soc.* **2009**, *131* (19), 6844−6854.

(21) Lee, C.; Keenan, C. R.; Sedlak, D. L. Polyoxometalate-enhanced oxidation of organic compounds by nanoparticulate zero-valent iron and ferrous ion in the presence of oxygen. *Environ. Sci. Technol.* **2008**, *42* (13), 4921−4926.

(22) de la Oliva, A. R.; Sans, V.; Miras, H. N.; Yan, J.; Zang, H.; Richmond, C. J.; Long, D.-L.; Cronin, L. Assembly of a Gigantic Polyoxometalate Cluster $\{W_{200}Co_8O_{660}\}$ in a Networked Reactor System. *Angew. Chem., Int. Ed.* **2012**, *51* (51), 12759−12762.

(23) Miras, H. N.; Yan, J.; Long, D. L.; Cronin, L. Structural Evolution of "S"-Shaped $[H_4W_{22}O_{74}]^{12-}$ and "§"-Shaped $[H_{10}W_{34}O_{116}]^{18-}$ Isopolyoxotungstate Clusters. *Angew. Chem., Int. Ed.* **2008**, *47* (44), 8420−8423.

(24) Granda, J. M.; Donina, L.; Dragone, V.; Long, D. L.; Cronin, L. Controlling an organic synthesis robot with machine learning to search for new reactivity. *Nature* **2018**, *559* (7714), 377−381.

(25) Raccuglia, P.; Elbert, K. C.; Adler, P. D. F.; Falk, C.; Wenny, M. B.; Mollo, A.; Zeller, M.; Friedler, S. A.; Schrier, J.; Norquist, A. J. Machine-learning-assisted materials discovery using failed experiments. *Nature* **2016**, *533* (7601), 73−76.